Marine Geology 404 (2018) 71–83

Contents lists available at ScienceDirect

Marine Geology

journal homepage: www.elsevier.com/locate/margo

Temporal and spatial variability in coastline response to declining sea-ice in northwest Alaska

L.M. Farquharson[a,*], D.H. Mann[b], D.K. Swanson[c], B.M. Jones[d], R.M. Buzard[b], J.W. Jordan[e]

[a] Geophysical Institute Permafrost Laboratory, University of Alaska Fairbanks, Fairbanks, AK, USA
[b] Department of Geosciences, University of Alaska Fairbanks, Fairbanks, AK, USA
[c] National Park Service, Fairbanks, AK, USA
[d] Water and Environmental Research Center, Institute of Northern Engineering, University of Alaska Fairbanks, Fairbanks, AK, USA
[e] Department of Environmental Studies, Antioch University New England, USA

ARTICLE INFO

Editor: E. Anthony

Keywords:
Arctic
Coastal erosion
Permafrost
Remote sensing
Sea-ice

ABSTRACT

Arctic sea-ice is declining in extent, leaving coastlines exposed to more storm-wave events. There is an urgent need to understand how these changes affect geomorphic processes along Arctic coasts. Here we describe spatial and temporal patterns of shoreline changes along two geomorphologically distinct, storm-wave dominated reaches of the Chukchi Sea coastline over the last 64 years. One study area encompasses the west- to southwest-facing, coarse-clastic shoreline and ice-rich bluffs of Cape Krusenstern (CAKR). The other covers the north-facing, sandy shorelines on barrier islands, ice-rich bluffs, and the Cape Espenberg spit in the Bering Land Bridge National Park (BELA). Both study areas lie within the zone of continuous permafrost, which exists both on and offshore and outcrops as ice-rich bluffs along the BELA coast. We mapped changes in coastal geomorphology over three observation periods: 1950–1980, 1980–2003, and 2003–2014 using aerial and satellite imagery. We then compared these geomorphic changes to changes in sea-ice coverage, which declined ~10 days per decade between 1979 and 2016 in the southern Chukchi Sea. Changes in coastal geomorphology in both BELA and CAKR exhibited high spatial variability over the study period. Between 2003 and 2014, shorelines of barrier islands in BELA exhibited the highest mean rates of change, $-1.5\ m\ yr^{-1}$, while coarse, clastic barrier beaches in CAKR showed only minimal change. Overall, shorelines in both BELA and CAKR became more dynamic (increasing erosion or increasing accumulation) after ca. 2003, with spatial variability in shoreline changes roughly doubling between the first period of observation (1950–1980) and the last (2003–2014). This increase in coastal dynamism may signal a transitional period leading to new state of geomorphic equilibria along these ice-affected coastlines.

1. Introduction

Approximately 34% of Earth's coastlines border Arctic seas above 60°N (AMAP, 2012; Lantuit et al., 2012). Despite being protected from wave action by the presence of sea-ice for 8 to 9 months of the year (Belchansky et al., 2004), some Arctic shorelines are markedly dynamic (Barnhart et al., 2014a; Jones et al., 2009). Warming climate, loss of permafrost, shifts in sediment supply, a decline in sea-ice cover and an increase in storms during the lengthening open water season (Lawrence and Slater, 2005; Stocker et al., 2014; Wang and Overland, 2009) threaten to trigger rapid and possibly drastic changes in coastal erosion and accretion in the Arctic over the coming century. Yet because of the cryosphere's nonlinear responses to climate change (Cohen et al., 2014; Miller et al., 2010; Serreze and Barry, 2011), and because of the nonlinear responses of coastlines to changing wave regimes (Komar, 1998; Stive et al., 2002), it is poorly understood how Arctic coastlines will respond to ongoing climate changes.

Sea-ice extent and duration, and onshore and offshore permafrost strongly influence Arctic coastal dynamics in space and time, specifically with respect to changing climate. Sea-ice is an important moderator of wave fetch and water temperature, and it shields coastlines from wave action, often for considerable portions of the year. The duration of sea-ice cover in the Arctic has declined by ~13% per decade since satellite observations began in 1979 (www.nsidc.org). Over the last ca. 40 years, the duration of landfast ice (ice seasonally frozen to the shoreface) in the Chukchi sea has declined one week per decade (Mahoney et al., 2014). The impact of sea-ice decline has already been observed through an increase in wave fetch, height, and swell size in

* Corresponding author at: Geophysical Institute Permafrost Laboratory, 2156 Koyukuk Drive, University of Alaska, Fairbanks, AK 99775, USA.
E-mail address: lmfarquharson@alaska.edu (L.M. Farquharson).

https://doi.org/10.1016/j.margeo.2018.07.007
Received 26 April 2018; Received in revised form 21 July 2018; Accepted 21 July 2018
Available online 23 July 2018
0025-3227/ © 2018 Elsevier B.V. All rights reserved.

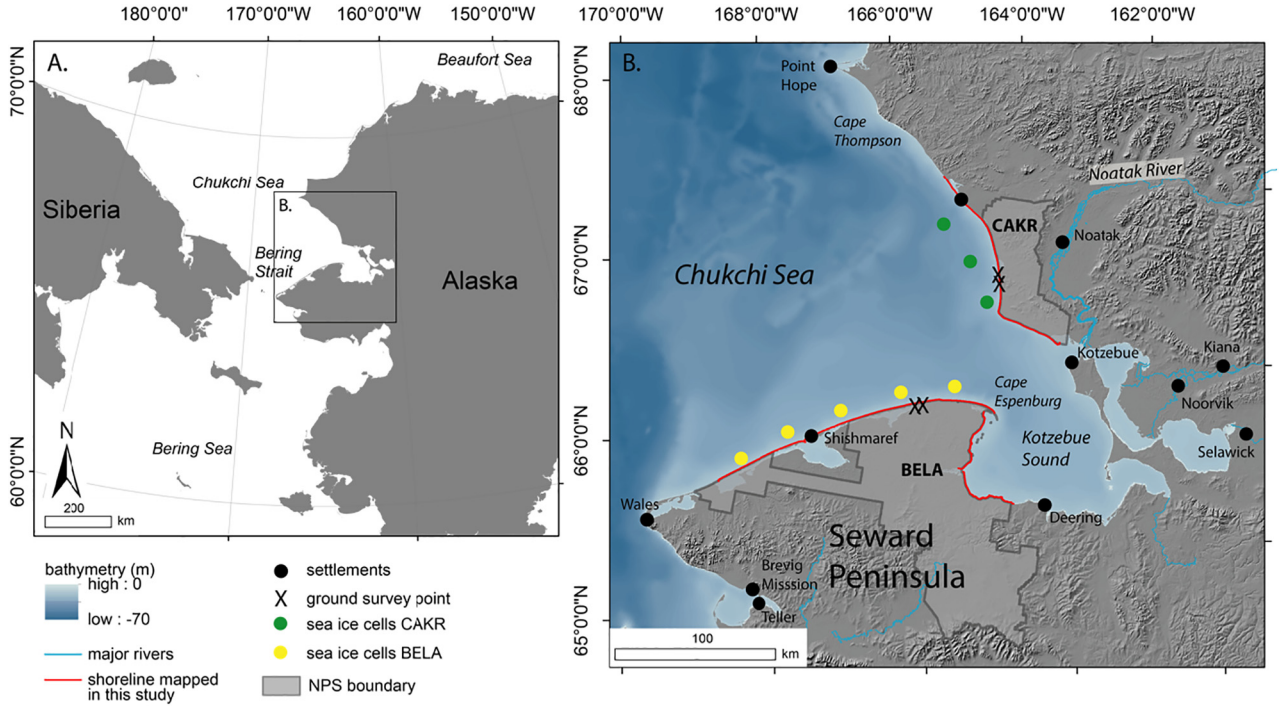

Fig. 1. The study region with Bering Land Bridge National Park and Preserve (BELA) and Cape Krusenstern National Monument (CAKR) outlined in grey.

Arctic seas (Francis et al., 2011; Overeem et al., 2011; Thomson et al., 2016; Thomson and Rogers, 2014), and the lengthening open-water season has resulted in increasing wave energy available for coastal erosion and sediment transport (Overeem et al., 2011). Another important effect of the changing sea-ice regime is the increased probability that autumn storms will make landfall before the winter ice has re-formed (Forbes, 2011). Storms occurring during the ice-free season generate the most geomorphologically significant wave events along Arctic coastlines and hence strongly influence coastal processes (Barnhart et al., 2014b; Mason et al., 1996).

Permafrost in the coastal zone affects shoreline geomorphic processes that occur over multiple temporal scales. Rising air and water temperatures are accelerating the thaw of permafrost, which is destabilizing some Arctic coastlines (Barnhart et al., 2014a; Günther et al., 2015; Kasprzak et al., 2017). Long term permafrost monitoring sites onshore in northern Alaska show an increase in temperature at 20 m depth of between 0.21 °C and 0.66 °C decade^{-1} between 1995 and 2015 (Romanovsky et al., 2017). Mean annual, ground temperatures in the Bering Land Bridge National Park and Preserve (BELA) are projected to increase by up to 3 °C by 2050 (Panda et al., 2016). Warming is also evident offshore where the sea-surface temperature (SST) of the Chukchi Sea has risen by 0.5 °C per decade since1982 (Timmermans and Proshutinsky, 2015). Among the potential impacts of permafrost thaw are more rapid erosion of ice-rich bluffs, which in some regions is already occurring with great rapidity (Jones et al., 2009). Another possible impact is an increase in sediment supply due to permafrost degradation along streams that supply sediment to barrier beaches, foredunes, spits and barrier islands that may now be sediment-poor.

Here we use repeat aerial and satellite imagery to estimate rates of shoreline change between 1950 and 2014 along two geologically distinct coastlines in the southeastern Chukchi Sea. Each study area contains several, distinctly different geomorphological subunits, and together encompasses 480 km of sea-ice affected coastline. We address these questions: 1) How variable have erosion and accretion been along these permafrost coastlines over the last 64 years? 2) Have different types of coastal geomorphology responded to sea-ice decline differently? 3) If ongoing trends in climate continue, how will these coastlines change over the coming centuries? By addressing these questions we provide new insight into coastal dynamics in the Chukchi Sea, a region whose geomorphic responses to ongoing climate change have been little studied compared to the Beaufort Sea coast.

2. Previous studies

The coastal dynamics of permafrost-affected shorelines have been studied primarily along the Beaufort Sea coast (Hume and Schalk, 1967; Jones et al., 2009; Jorgenson and Brown, 2005; Mars and Houseknecht, 2007), the Beaufort Sea coast of Canada (Harper, 1990; Hequette and Barnes, 1990; Lantuit and Pollard, 2008; Radosavljevic et al., 2016; Solomon, 2005), and the Arctic seas of Siberia (Günther et al., 2015, 2013). Much of this research has focused on the often spectacular erosion of ice-rich permafrost bluffs (e.g., MacCarthy, 1953; Jones et al., 2009; Günther et al., 2015), and to a lesser extent on the dynamics of Arctic barrier-island systems (Gorokhovich and Leiserowiz, 2012; Harper, 1990; Hequette and Ruz, 1991). Only a few studies (including Hequette and Ruz, 1991 and Radosavljevic et al., 2016) have explored how permafrost-affected Arctic coastlines of mixed morphology and grain size respond to sea-ice decline and permafrost thaw.

Previous studies of coastal dynamics in the southeastern Chukchi Sea measured rates of coastal change between 1950 and 1980 using the "instantaneous water line." This is the position of the land–water interface when a remote-sensing image is acquired (Boak and Turner, 2005) and is used as an estimate of shoreline position (Manley et al., 2007). Mean rates of change in the instantaneous water line along the BELA and CAKR coastlines suggested an overall erosional trend between 1950 and 1980, followed by an overall accretional trend between 1980 and 2003 (Gorokhovich and Leiserowiz, 2012). Defining shoreline position based on instantaneous water lines is problematic in a place like the Chukchi Sea where relative sea level can change by > 1 m in response to short-lived storm surges. Despite the low tidal range of approximately 25 cm (tidesandcurrents.noaa.gov), we observed that the gently sloping beaches of BELA allow the water line to shift landward by several meters during an average diurnal cycle.

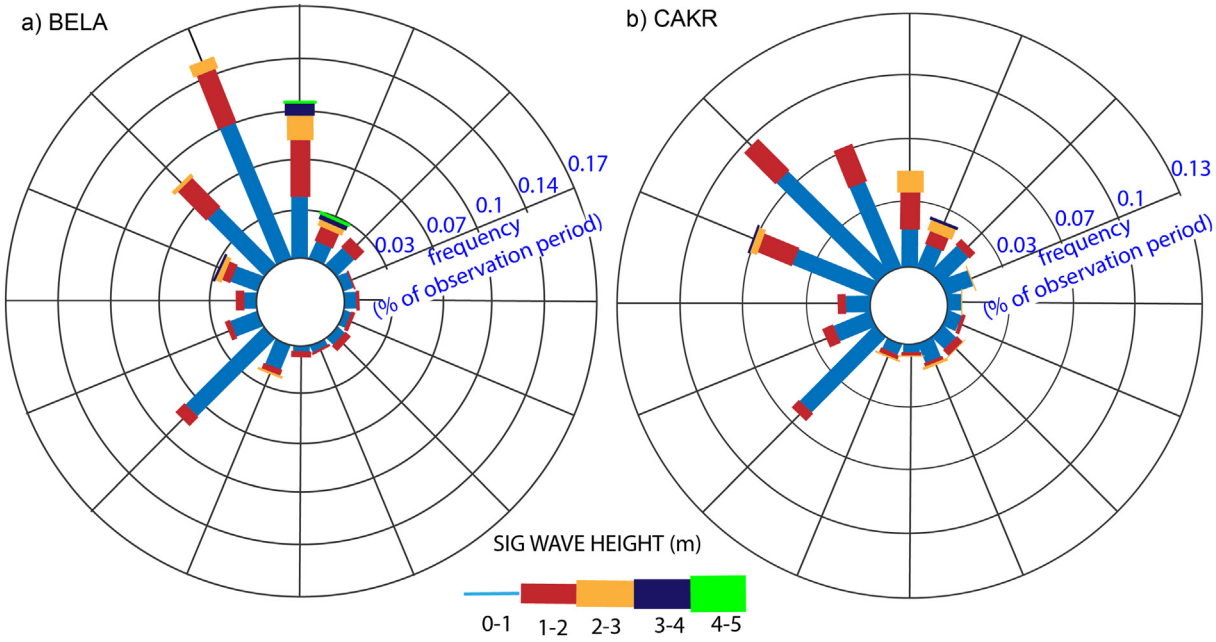

Fig. 2. Directions of wave approach and significant wave height along the BELA and CAKR coastlines during 2014. Modified from http://wis.usace.army.mil/.

3. Study area

3.1. Climate and weather

BELA and CAKR are located between 65° and 67°N and comprise the shores of Kotzebue Sound and the southeastern Chukchi Sea (Fig. 1). The region is situated within a zone of continuous permafrost and has a mean July air temperature of 13 °C, a mean annual temperature of −5 °C, and mean annual precipitation of 25 cm (NCDC 1981–2010 monthly normals for Kotzebue, http://www.wrcc.dri.edu/). In both BELA and CAKR, the predominant wave approach is from the NW (Fig. 2) (http://wis.usace.army.mil). Wave heights during the ice-free season average 0.9 and 0.8 m along the BELA and CAKR shorelines, respectively (http://wis.usace.army.mil/). A NOAA tidal gauge is located in the north of CAKR, and the annual, mean tidal range at this site is 25 cm (tidesandcurrents.noaa.gov/).

Despite the Chukchi Sea's micro-tidal regime, RSL can change up to 4 m in response to storm surges (Blier et al., 1997; Fathauer, 1978). Most storms arrive from the Arctic Ocean in the form of polar lows (Rasmussen et al., 2004) and the waves generated by these storms during the ice-free period are the primary drivers of coastal sedimentary and erosional processes in both BELA and CAKR. Storm intensity in the Chukchi Sea peaks in the autumn and winter (Mason et al., 1996) when low-pressure systems can generate waves reaching > 10 m (https://www.ncdc.noaa.gov/stormevents/). Shallow water depths of 20 m or less extend 15–25 km offshore (Fig. 1) and contribute to the intensification of the resultant storm surges.

3.2. Sea-ice

In the southern Chukchi Sea, sea-ice typically forms in mid-November and persists until mid-June, leaving only five months of open water on average (NSIDC, http://nsidc.org/data). Landfast ice expands seaward beginning in October, eventually extending up to 10 km offshore in CAKR and 50 km in BELA. Landfast ice begins to retreat rapidly in May, and in most years has disappeared by mid-July (Mahoney et al., 2014).

3.3. Coastal geomorphology

The present coastline was established between 5000 and 3000 years BP when relative sea level (RSL) stabilized after rising in postglacial times to submerge the Bering Land Bridge (Hopkins, 1973; Elias et al., 1996; Mason et al., 1995). Some coastal landforms, including barrier islands in BELA and CAKR formed as recently as 1700 years BP (Jordan and Mason, 1999).

Both BELA and CAKR are micro-tidal, ice-affected, and wave-dominated coasts, but their coastal geomorphology differs markedly. The CAKR coastline consists of a coarse-clastic, cuspate spit enclosing Krusenstern Lagoon; its accretionary beach ridges were built by longshore transport of sediments derived from the erosion of rocky uplands and stream deposits to the north (Hopkins, 1977). In contrast, the BELA coastline is low-lying and dominated by longshore drift from the southwest that reworks sand and silt into barrier islands and into the recurved spit of Cape Espenberg (Farquharson et al., 2016; Lenz et al., 2016). As detailed below, BELA and CAKR are geomorphologically diverse and consist of a mixture of barrier island systems, spits, foredune plains, and ice-rich permafrost bluffs (Fig. 3). As such, they provide an opportunity to explore how two geographically diverse, Arctic coastlines respond to similar changes in sea-ice regime and temperature.

3.3.1. Bering Land Bridge National Park (BELA)

The sand-dominated BELA coastline (Figs. 1, 3) is composed of two reaches, one facing northwest into the Chukchi Sea, and the other facing northeast into Kotzebue Sound. Along the northwest-facing shoreline, wave fetch exceeds 500 km during the ice-free season and the predominant wave direction is from the NW (Fig. 2). In contrast, maximum fetch along the east-facing shoreline of BELA in Kotzebue Sound is ~100 km. Offshore of BELA, bathymetry is shallow and gently sloping, and the 20-meter isobath lies 10 and 50 km offshore. Along the BELA coastline, wave set-up during storms creates surges up to 4 m high, which can overwhelm micro-tidal variations (Blier et al., 1997; Fathauer, 1978). The coastal geomorphology of BELA is a mixture of barrier lagoon systems, ice-rich permafrost bluffs, aggrading spits, and estuaries (Fig. 3). Shallow nearshore bathymetry, onshore storms, and west to east long-shore drift have facilitated the late Holocene deposition of the Cape Espenberg beach ridge plain and its 0.5–3 km wide

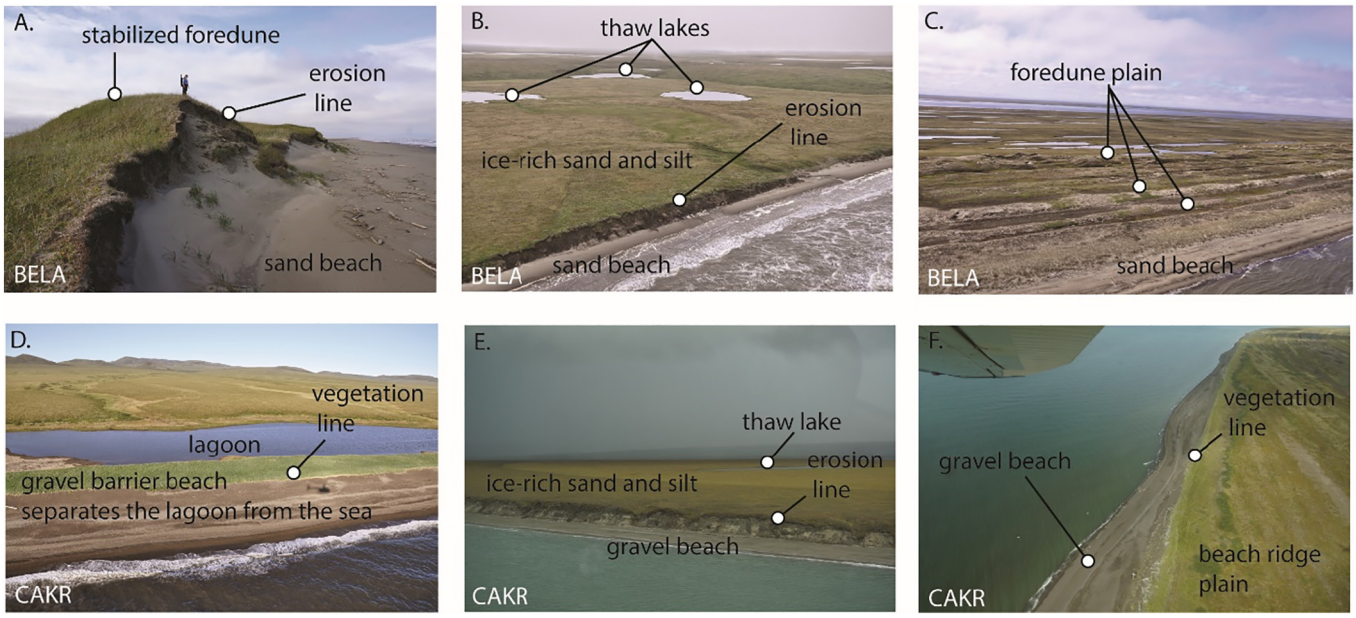

Fig. 3. Coastal geomorphology in the study areas. A) Stabilized and eroding foredunes in BELA, person for scale. B) A thawing ice-rich permafrost (yedoma) bluff in the southwest reach of the BELA study area. C) Foredunes on the Cape Espenburg spit in BELA. D) Gravel barrier beach separating a lagoon from the sea in CAKR. E) Permafrost bluffs in CAKR fronted by gravel shoreface. F) Gravel beach and beach-ridge plain at Cape Krusenstern.
Images B, C, D, courtesy of NOAA Shorezone (www.shorezone.org).

offshore sand bars, which are conspicuous east and south of the tip of Cape Espenberg in Kotzebue Sound (Fig. 1).

The northwest-facing shoreline of BELA contains three large lagoon systems, which reach over 400 km^2 in size and are separated from the sea by low-lying barrier islands 5 to 50 km in length. The wide and gently sloping sandy shorefaces of these barrier islands act to dissipate wave energy. Lagoon backshores are formed by ice-rich, permafrost bluffs that are dissected by numerous streams. Salt marshes are widespread in back-barrier areas at levels ~1 m above sea level. Infilled washover channels, abandoned floodtide deltas, former tidal inlets, and relict en echelon foredunes provide evidence of shifts in the locations of tidal inlets (Jordan and Mason, 1999; Mason et al., 1997). Inland of the coast is a tundra lowland dotted with thermokarst lakes and drained thermokarst lake basins underlain at shallow depths by ice-rich permafrost (Farquharson et al., 2016; Lenz et al., 2016). The predominant sediment in these lowlands is organic-rich silt (yedoma).

3.3.2. Cape Krusenstern National Monument (CAKR)

In contrast to the sandy shorelines in BELA, CAKR shorelines are gravel dominated and consist of two reaches differing in aspect, one facing west and the other southwest (Fig. 1). The fetch on the west-facing coastline can be > 500 km during the open-water season, and waves arrive predominantly from the NW (Fig. 2). The fetch on the southwest-facing shoreline is less, reaching a maximum of just 100 km. Offshore, bathymetry is characterized by a slightly steeper gradient than at BELA (Fig. 1).

The coastal geomorphology of CAKR is dominated by gravel barrier beach ridges backed by 3–6 m high permafrost-rich bluffs. The southern flank of the cuspate spit enclosing Krusenstern Lagoon consists of a broad, beach-ridge plain (Fig. 3). The lagoons are isolated from the sea except in spring when ephemeral channels form during break-up. The backshores of these lagoons consist of vegetated, permafrost bluffs. (Fig. 3d). Cape Krusenstern Lagoon is large enough (30 km^2) to experience wave action sufficient to build an internal set of prograding beach ridges along its shore (Mason and Jordan, 1993).

4. Methods

4.1. Data set description

We assessed coastal change along 480 km of shoreline, including 340 km in BELA and 140 km in CAKR, using ortho-rectified aerial imagery acquired in 1950, 1980, and 2003 (Manley et al., 2007a, 2007b, 2007c). In addition, we acquired panchromatic and multispectral WorldView-2 satellite imagery from 2014, which was ortho-rectified using a 2012 IfSAR-derived digital surface model and then georeferenced to the 2003 aerial images of Manley et al. (2007c) following the procedures of Manley and Lestak (2012).

4.2. Shoreline digitization and measuring change

To estimate shoreline changes, we mapped erosion scarps (ES) wherever they were visible. An ES is the topographic break between the permafrost bluff, beach ridge, or foredune and the beach (Boak and Turner, 2005). We chose to map this feature because it was visible in all the remote sensing images and was present along significant portions of the coastline. The main issue with using the ES, is that like other, non-datum related proxies of shoreline position it indicates where erosion is occurring, and only rarely allows for measurement of deposition (Boak and Turner, 2005). In cases where an ES was not visible in the imagery, we mapped the seaward edge of vegetation where it was obviously controlled by high water and clearly marked by abrupt spectral differences between vegetated and unvegetated surfaces (Boak and Turner, 2005). If the vegetation line was diffuse, the area was not included in the mapping.

Once the shoreline was mapped for all observation periods (1950, 1980, 2003, 2014), we calculated rates of shoreline change using the U.S. Geological Survey Digital Shoreline Analysis Tool, (DSAS, Thieler et al., 2009) in 50-m long shoreline segments between each time step. Measurements were only possible in segments where the ES was clearly identifiable on both imagery dates. In some cases, notably in the cases of interdune areas and salt marshes, an ES was not present and was therefore not mapped.

We compared variation in erosion rates between imagery dates

Table 1
Annualized errors for each shoreline and time slice, given in m yr^{-1}.

	1950–1980	1980–2003	2003–2014
BELA	0.13	0.13	0.14
CAKR	0.11	0.12	0.19

using an F test of equality of variances. To account for spatial autocorrelation among adjacent transects, we constructed variograms using the R 'sm' package (Bowman and Azzalini, 2014; R Development Core Team, 2016). We then inspected the variograms of the end-point rate for the range (the distance at which spatial autocorrelation becomes negligible) (Bowman and Crujeiras, 2013). Over most of the study area, we found the range was < 1 km (20 transects at 50 m spacing) but that occasionally it was as much as 2 km (40 transects at 50 m spacing). Following Lentz et al. (2013), we then reduced the F-test's degrees of freedom, n (the number of transects), to (n / 40) − 1 to compensate for this level of spatial autocorrelation. Similarly, when testing for differences in annual mean rate of erosion between imagery dates, we used a paired *t*-test with degrees of freedom reduced by a factor of 40. Error estimates for erosion rates were calculated following Eq. (1):

$$Error\frac{m}{yr} = \frac{\sqrt{(E_{p1})^2 + (E_{p2})^2 + (RMS_1)^2 + (RMS_2)^2}}{\Delta t} \quad (1)$$

where Ep1 and Ep2 represent the pixel resolution of the imagery, RMS1 and RMS2 are the root mean square errors from the geo-registration of each image, and Δt is the duration in years of each time step (Jones et al., 2009). Errors for each observation period are listed in Table 1.

To explore the drivers of coastal dynamics, we compared coastal dynamics between BELA (sand-dominated) and CAKR (gravel-dominated) and classified the shoreline according to supratidal-zone geomorphology (Table 2). Coastal geomorphology classes in BELA include foredunes, non-foredune (barrier) and in CAKR include gravel barriers and beach ridges. Permafrost bluffs were mapped in both study areas.

4.3. Ground-truthing

To check the accuracy of our digital mapping, we conducted field surveys during the summer of 2015 along 40 km of coastline (20 km in each of BELA and CAKR). In addition, we did low-elevation aircraft flights along 150 km of the BELA coastline and 60 km of the CAKR coastline. While digitally mapping, we frequently referred to the oblique coast photographs provided by the Alaska Shorezone Coastal Mapping and Imagery tool (NOAA https://alaskafisheries.noaa.gov/mapping/szflex/). We also utilized the long-term shoreline transects established by Jordan in 1987 (pers. Comm) and conducted additional measurements at five of their sites (three in BELA and two in CAKR) during the summer of 2015 (for locations, see Fig. 1). At each long-term monitoring site visited we measured from permanently installed survey markers to the edge of the permafrost bluff, beach ridge, or foredune. These field measurements closely matched our remote sensing measurements (R^2 = 0.74) with a maximum offset of ± 0.12 m yr^{-1}, which we attribute to spatial variability in erosion along the shore (see Table S2).

Table 2
Geomorphology classes and their distribution.

CAKR	Beach ridges	Welded gravel bar	Permafrost bluff
Length of shoreline (km)	32.85	58.40	52.15
Percent of shoreline	22.91	40.73	36.37

BELA	Foredune (barrier)	Non-foredune (barrier)	Permafrost bluff
Length of shoreline (km)	165.45	63.30	115.35
Percent of shoreline	48.08	18.40	33.52

4.4. Sea-ice data

We obtained daily and bi-daily sea-ice concentrations for the period 1979 to 2016 based on Nimbus-7 SMMR and DMSP SSM/I-SSMIS Passive Microwave Data from the National Snow and Ice Data Center (http://nsidc.org/data/nsidc-0051). Five representative, 25-km^2, nearshore pixels were analyzed for BELA and three for CAKR (for locations see Fig. 1). Sea-ice concentrations < 15% were considered "open water", assuming that sea-ice at or above this concentration would dampen waves (Overeem et al., 2011). The first, last, and total number of open-water days per year for each site's sampled pixels were averaged to analyze annual changes in open water. Missing days were interpolated to keep this measure consistent.

Mean daily fetch was calculated for each site using the same NSIDC dataset. From (but not including) each sampled pixel, 250 km-long bearings were cast at 10° intervals onto land-free regions. For each day, the distance of unimpeded open water from the starting pixel was measured along each bearing. The mean daily fetch of all site pixels was combined to give an overall estimate of fetch. This method weighs mean daily fetch by the frequency of available full-length vectors reaching the coast, and is thus less susceptible to outliers than the more commonly used, single-bearing method.

5. Results

5.1. Open water season

Analysis of trends in the seasonal coverage of nearshore sea-ice show the open water season has increased by ~10 days per decade for both BELA and CAKR since 1979 (Fig. 4a, b). In 2016, sea-ice breakup occurred approximately two weeks earlier than it had in 1979, and sea-ice formation in autumn occurred approximately six weeks later than in 1979. Trends in sea-ice decline are similar for both study areas, though BELA exhibits a slightly greater increase amounting to two days per decade.

The presence of sea ice controls maximum fetch for the shorelines in both study areas, and between 1979 and 2016 the time interval when fetch was > 250 km increased at both the beginning and end of the open water season (Fig. 4c). Importantly, the largest changes in maximum fetch for both BELA and CAKR have coincided with the autumn storm season (black bars in Fig. 4c). This means that storms are now more likely to occur during the open-water season when there is sufficient fetch for geomorphologically-significant waves to develop.

5.2. Coastal erosion and accretion along different shoreline types

Remote sensing data and ground-based observations indicate that several different erosion processes are occurring, some of which are specific to particular shoreline types. Erosion along permafrost bluffs is primarily caused by thermo-abrasion (thermal and mechanical erosion of permafrost by waves) and by thermo-denudation (thaw of sub-aerially exposed permafrost) (Are, 1988). Numerous thermoerosion gullies developed in permafrost bluffs backing the BELA coastline between 2003 and 2014 and contributed to the erosion of these bluffs.

In contrast to permafrost bluffs, coastal dynamics along the barrier islands in BELA does not involve obvious thermo-erosion, but instead consists of three main processes that also occur widely on non-permafrost coastlines at lower latitudes: i) undercutting of foredune fronts, ii) formation of overwash fans during storms, and iii) aeolian transport of shoreface sediment inland across the barrier island.

Accretion within BELA was confined to the Cape Espenberg spit. Although the absence of wave-modified vegetation lines made it

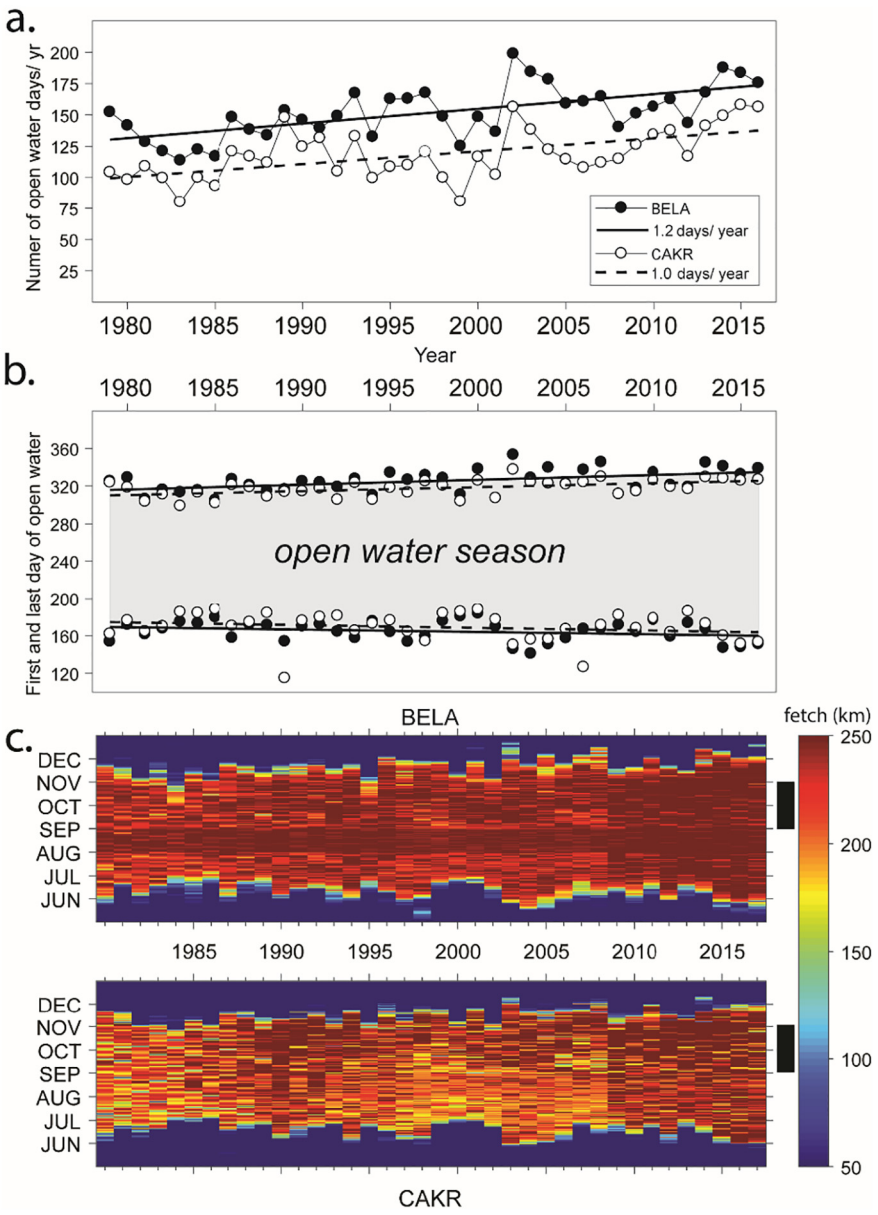

Fig. 4. Changes in sea-ice cover and resultant fetch in the study areas between 1979 and 2016 for locations shown in Fig. 1, using the methodology of Cavalieri et al. (1996). A longer ice-free season since 1979 has caused an increase in the amount of time each summer when fetches exceed 200 km. A) Number of open water days in BELA (closed circles) and CAKR (open circles). For BELA the regression line equation is $y = 1.17 - 2183.29$, $r^2 = 0.40$, for CAKR $y = 1.03x - 1937.37$, $r^2 = 0.33$. B) First (spring) and last (fall) open water days for BELA (closed circle) and CAKR (open circle). For BELA the first day of open water season regression line equation is $y = -0.25x - 665.26$, $R2 = 0.07$, the last day $y = 0.51x - 700.82$, $R2 = 0.23$. For CAKR, first day of the open water season regression line is $y = -0.29x - 750.32$, $R2 = 0.04$ and the last day, $y = 0.42x - 520.93$, $R2 = 0.27$. C) Variations in fetch for BELA (top) and CAKR (bottom) with red indicating that the fetch exceeds 250 km. Black bars to the right of the plot indicate the timing of the fall storm season. See Fig. S3 for maps of the grid points used for fetch analysis. The abrupt color contrast in 2008 is due to a change in sensor from SSM/I (1987–2007) to SSMIS (2008-current). (For interpretation of the references to color in this figure legend, the reader is referred to the web version of this article.)

difficult to precisely map accretion along the spit, the time series of imagery does reveal progressive welding of longshore sand bars onto the accreting face of the extending spit (Fig. 3c).

Accretion in CAKR was more widespread and obvious than in BELA. Along the ocean shore of Cape Krusenstern, seaward movement of the vegetation line is consistent with ongoing beach accretion. During T3 (2003–2014), maximum rates of accretion were between 1.3 and 3 m yr^{-1} along this shoreline.

5.3. Spatial and temporal patterns of shoreline change

Rates of coastal change varied widely between the two study areas and during different observation periods (Figs. 5–8). In BELA, mean rates of change were -0.68 m yr^{-1} during T1 (1950–1980), -0.26 m yr^{-1} during T2 (1980–2003), and -0.68 m yr^{-1} during T3 (2003–2014) (Table 3) (negative values indicate erosion). In CAKR, mean rates of change were -0.04 during T1 (stable when errors are taken into account), -0.22 m yr^{-1} during T2, and -0.13 m yr^{-1} during T3 (Table 3). Overall, the sandier shorelines in BELA had higher rates of change.

The variance in the rate of change in ES line position along the transects provides an indicator of the spatial variability of coastal change rates. Variance was higher during T3 than during either T1 or T2 in both BELA and CAKR (Tables 3 and 4). F-tests indicate these differences were statistically significant ($p < 0.05$) in all cases (Table 4). Along with the variance, the widest range in rate-of-change values occurred in recent years (2003–2014) along both shorelines. In BELA, the range in rates of change during each survey interval was 2.59 m yr^{-1} during T1, 2.01 during T2, and 4.79 during T3. In CAKR they were 3.34 m yr^{-1} during T1, 3.83 during T2, and 6.54 during T3 (Table 3).

There are potential problems with comparing variances in rates of change that are estimated from observation periods with different durations (T1 30 yr, T2 24 yr, and T3 11 yrs) (Dolan et al., 1991). The most variable observation period (2003–2014) is also the shortest one. To explore this issue further, we compared the variance in ES-rate-of-change to the durations of observation periods for all possible pairs of sample dates (1950–1980, 1950–2003, 1950–2014, 1980–2003, 1980–2014, and 2003–2014) using only those transect points having values for all three observation periods (n = 562 and n = 373 in BELA

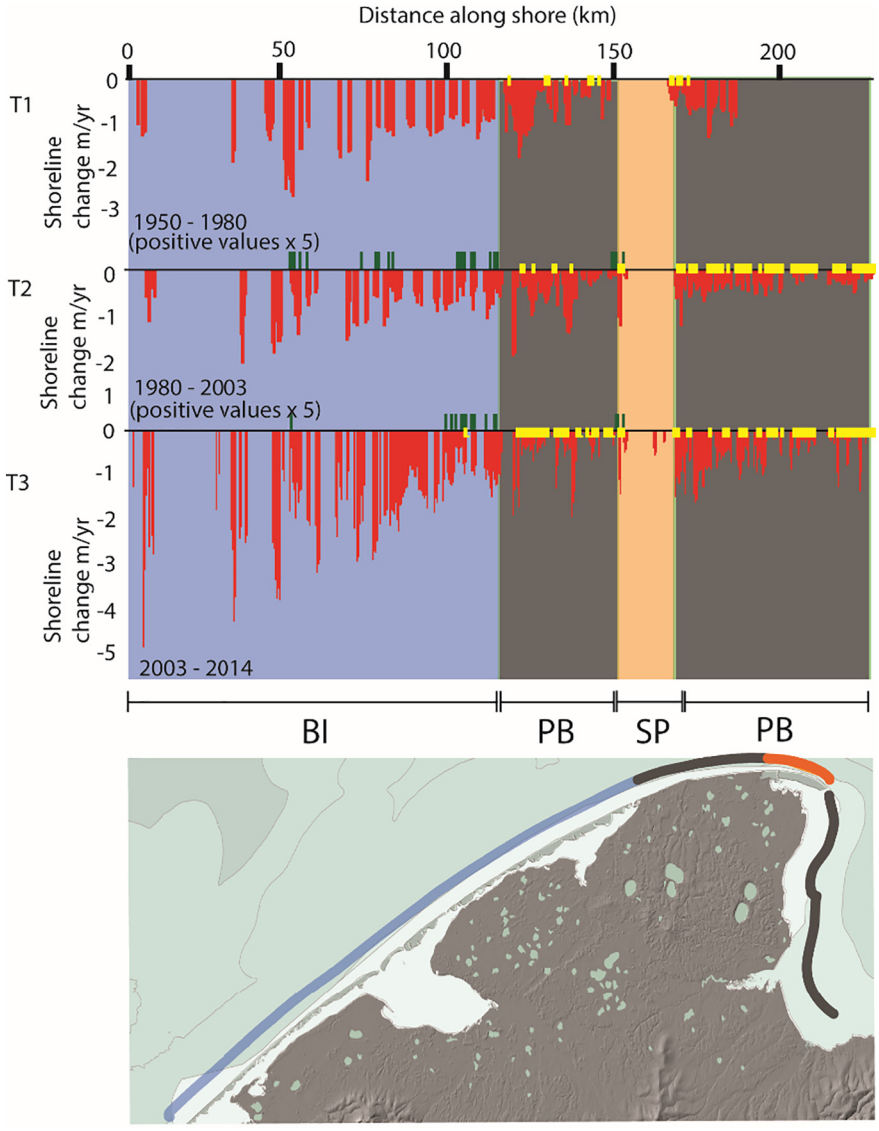

Fig. 5. Shoreline changes ($m\,yr^{-1}$) in BELA during the three study periods: A. 1950–1980, B. 1980–2003, C. 2003–2014. Each histogram column depicts a transect across the shoreline. Red bars indicate erosion; green bars/points indicate accretion. In T1 and T2, green bar height is increased 5× to make them more visible. Yellow dots represent transects which were measured, but where no change was observed. Transects are arranged from southwest to northeast. Background shading corresponds to the color of the main coastal reaches shown on the map: blue = barrier island; grey = permafrost bluff; orange = spit. (For interpretation of the references to color in this figure legend, the reader is referred to the web version of this article.)

and CAKR, respectively). In both BELA and CAKR, the variability noted during all observation periods was similar, except for the most recent one. Observation periods that differ greatly in length show quite similar variability. For example, sample variance was 0.15 in BELA for the both the 64-year (1950–2014) and the 34-year (1980–2014) observation periods (Table S1). Similarly in CAKR, sample variance was 0.07 and 0.09 for the 64-year (1950–2014) and the 34-year (1980–2014) observation periods, respectively (Table S1). We conclude that the recent increase in sample variance in T3 is real and not an artefact of observation-period length.

The rate of shoreline change varied widely in BELA and CAKR over the course of the three observation periods (Figs. 5–8). Mean rates of change in BELA were highest ($-0.68\,m\,yr^{-1}$) during T1 and T3 (Table 3). CAKR consistently experienced lower change rates, and interestingly showed the highest mean rate of change during T2, $-0.22\,m\,yr^{-1}$, compared to $-0.04\,m\,yr^{-1}$ during T1 and $-0.13\,m\,yr^{-1}$ during T2 (Table 3). Paired *t*-tests showed that the mean differences between T3 and the previous observation periods were significant only in BELA during T3 compared to T2 (Table S3).

5.4. Rates of shoreline changes in different geomorphic settings

Erosion rates have varied alongshore and between different types of coastal geomorphology. Within BELA, a clear erosion gradient exists as a consequence of longshore drift transporting sediment from the SW to the NE. Along this north-facing barrier-lagoon system (Fig. 1), an increase in offshore storm wave energy enhanced by a longer open water season and onshore permafrost degradation seems to be driving the more rapid shoreline erosion. (Fig. 5). At the same time, accretion has occurred downdrift to the northeast on Cape Espenberg (Fig. 6). This pattern has been accentuated over time, with T3 (2003–2014) exhibiting the strongest alongshore gradient in erosion rates.

Within BELA, shorelines associated with barrier islands have experienced the greatest variations, with mean rates of change up to $-1.53\,m\,yr^{-1}$ occurring between 2003 and 2014 along low-relief reaches of coast lacking foredunes in the supratidal zone. During T1, T2, and T3, mean rates of shoreline change in areas lacking foredunes were $-0.82\,m\,yr^{-1}$, $-0.59\,m\,yr^{-1}$, and $-1.53\,m\,yr^{-1}$, respectively (Table 3). Along sections of coast with foredunes in the supratidal zone, change occurred at lower rates: $-0.86\,m\,yr^{-1}$, $0.34\,m\,yr^{-1}$, and $0.93\,m\,yr^{-1}$ for T1, T2 and T3, respectively (Table 3). Interestingly, shorelines backed by foredunes along the BELA coast exhibited the maximum rates of change observed anywhere in the study: $-4.79\,m\,yr^{-1}$ during T3. In contrast, ice-rich permafrost bluffs eroded more slowly, with a maximum change rate of only $-0.51\,m\,yr^{-1}$ between 1950 and 1980. Over the course of T1, T2, and T3, mean rates of

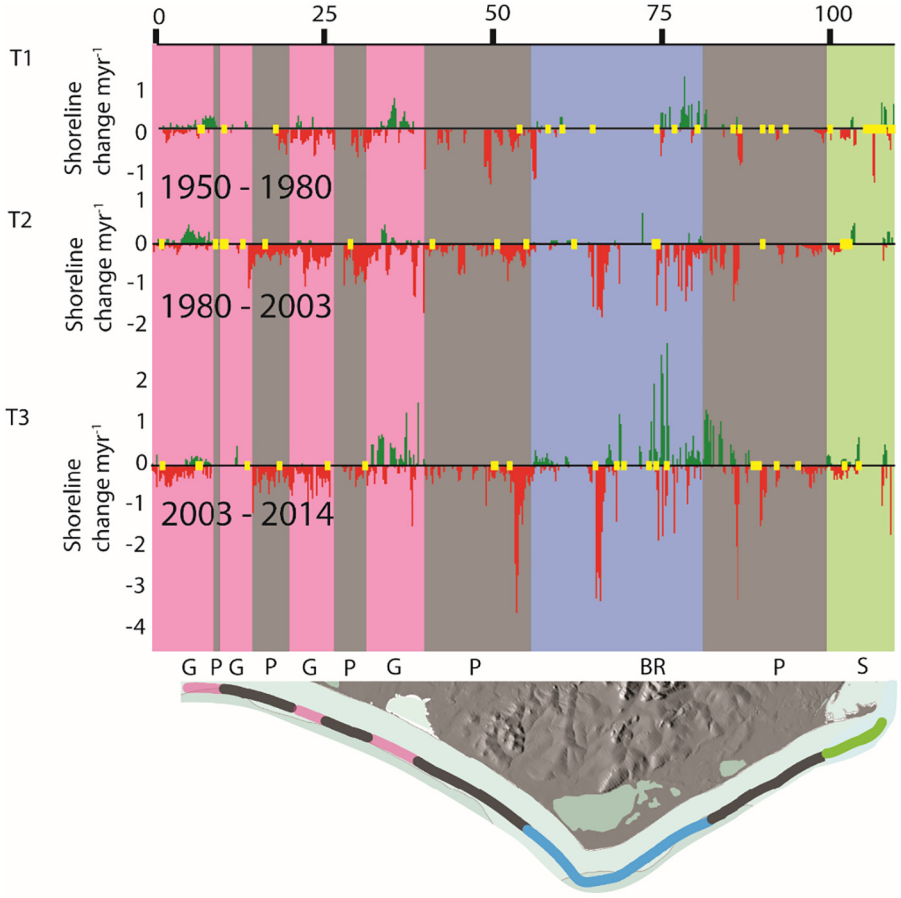

Fig. 6. Shoreline change (m yr^{-1}) in CAKR during each of the three study periods: T1, 1950–1980, T2, 1980–2003, and T3 2003–2014. Each histogram column depicts a transect point along shore. Yellow dots show where change was measured at 0 m yr^{-1}. Transects are arranged northwest to southeast. Colors in the background correspond to the main types of coastal geomorphology: pink = gravel bars; grey = permafrost bluffs; blue = welded gravel bars and beach ridges; green = spit. (For interpretation of the references to color in this figure legend, the reader is referred to the web version of this article.)

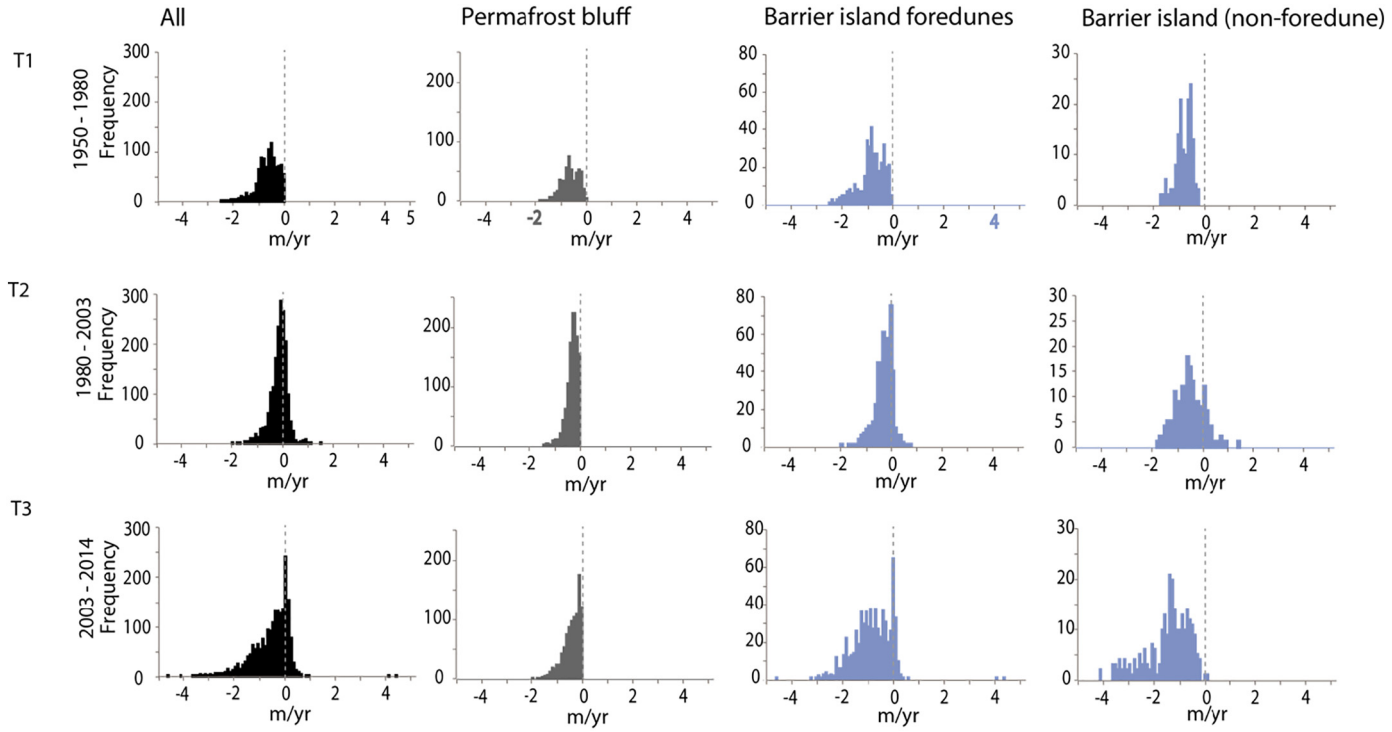

Fig. 7. Rates of shoreline changes in BELA for the main geomorphic landforms present there during T1, 1950–1980, T2, 1980–2003, and T3 2003–2014. Data are binned in 0.1 m yr^{-1} increments.

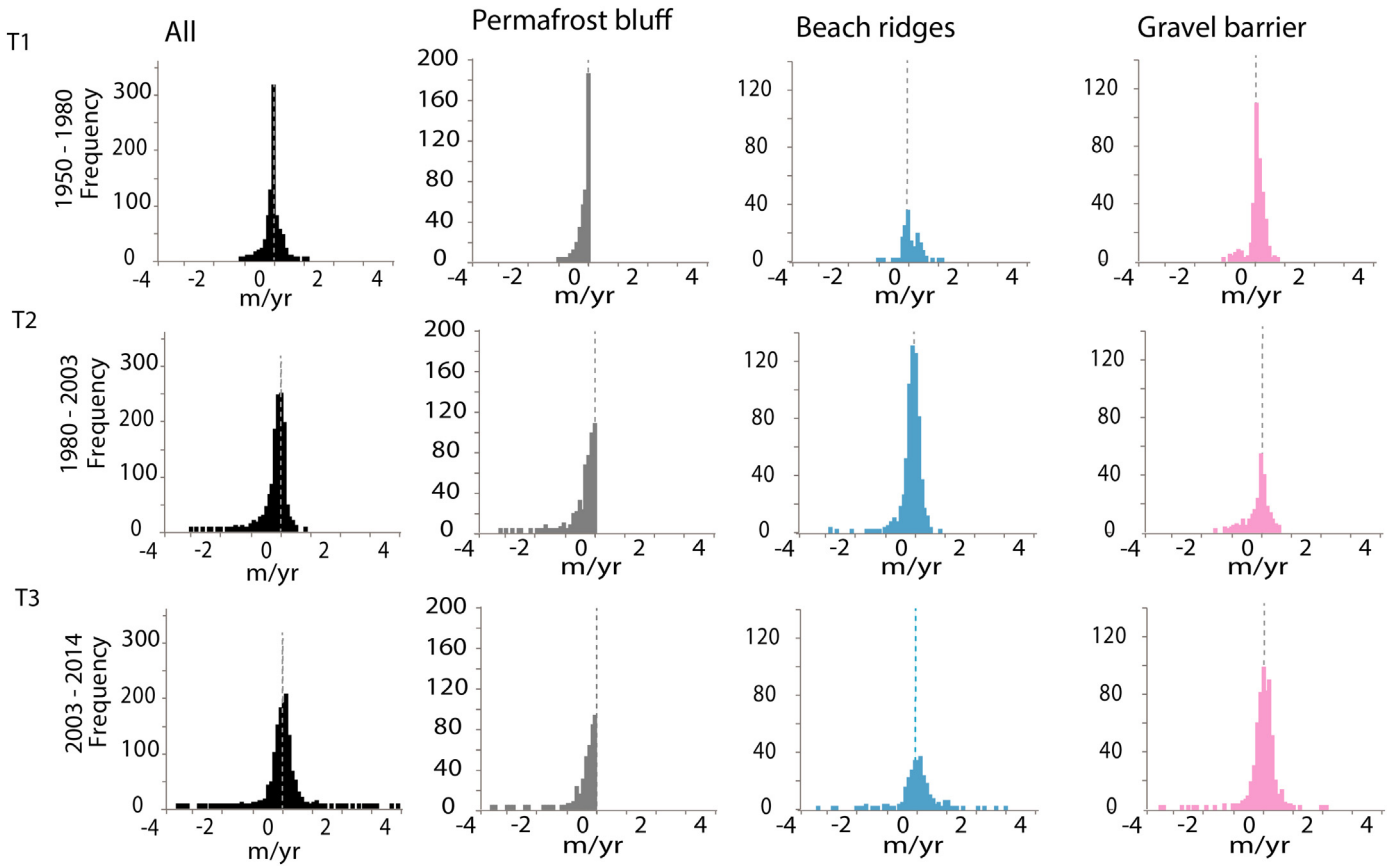

Fig. 8. Rate of shoreline change in CAKR for the main classes of coastal geomorphology. A) 1950–1980, B) 1980–2003, C) 2003–2014. Data are binned in 0.1 m yr^{-1} increments.

change along permafrost bluffs were -0.51 m yr^{-1}, -0.18 m yr^{-1}, and -0.32 m yr^{-1}, respectively.

In CAKR, the spatial distribution of rates of shoreline change has been more complex than in BELA, and no long term alongshore gradient in erosion/accretion rates was observed. Sediment deposition and shoreline progradation occurred mainly on the outer shore of Cape Krusenstern lagoon where both erosion and accretion were most rapid during T3, and slower during both T1 and T2. Overall, permafrost bluffs exhibited the highest mean change rates (-0.16, -0.30 and -0.20 yr^{-1} for T1, T2, and T3 respectively) of anywhere in the CAKR study area, yet the maximum rates of change (-3.57 m yr^{-1}) were observed along shorelines backed by beach-ridge plains adjacent to tidal inlets (Fig. 3d) during observation period T3.

6. Discussion

6.1. Observed changes in coastal dynamics at BELA and CAKR

Since 2003, coastlines in the southern Chukchi Sea have become more dynamic compared to the previous 53 years in terms of both shoreline erosion and accretion. A likely cause is the increase of ~10 days per decade in the open-water season and the corresponding increase in the time available for wave energy to do geomorphic work along these shorelines.

The increase in erosion rates has not occurred in a linear fashion. In BELA, erosion rates and the variance in these rates were high between 1950 and 1980, lower between 1980 and 2003, and then increased to their highest values between 2003 and 2014. In contrast, CAKR experienced highest rates of shoreline change between 1980 and 2003. One possible, but so far untested explanation for this fluctuating, upward trend in erosion rates is change in the frequency and intensity of storms (Barnhart et al., 2014a).

As Lantuit et al. (2012) point out, changes in subtidal permafrost can play crucial roles in determining geomorphic changes onshore. We have no information on changes in the subtidal zone of the study areas that may have occurred simultaneously with changes in the intertidal and supratidal zones there. A distinct possibility exists that subtidal, nearshore features such as sand bars may be responding more rapidly to changes in wave-climate than the subaerial landforms mapped in this study.

6.2. Geomorphology, geology and exposure drive variability in erosion rates

Shorelines in BELA and CAKR have responded differently to changes in sea-ice conditions during the past 64 years. CAKR shorelines have been less affected than those in BELA, both in terms of the variance and the mean rate of shoreline change. This difference may be due to several factors. First, the sandy beaches and foredunes of BELA require less energy for sediment transport and erosion than those of the CAKR shoreline. Second, the barrier island and spit shorefaces in BELA are less steep, which enables wave energy to travel further onshore. Third, the orientation of the BELA coastline allows the predominately northwesterly winds to set up east-flowing longshore drift. Forth, BELA's northerly aspect creates a fetch > 1000 km during summer months, with the seasonal window for this large fetch increasing as sea-ice cover has declined. In contrast, CAKR shorefaces are steeper and composed of coarser sediment that requires more wave energy to erode or transport, and typical fetch at CAKR is only ca. 300 km due to its predominately westerly aspect.

Table 3
Summary statistics for all times slices for BELA and CAKR. Abbreviations for shoreline types are as follows: PB, permafrost bluff; BI, barrier island; FD, foredune; GB, welded gravel bar; BR, beach ridge. Note that the variances in Table 4 differ slightly from those in this table because the values in Table 4 include only those transects with data available for both time slices. Negative values indicate erosion.

Study site 1: BELA	1950 to 1980				1980 to 2003				2003 to 2014			
	ALL	PB	BI	FD	ALL	PB	BI	FD	All	PB	BI	FD
Ice content	N/A	High	Low	Low	N/A	High	Low	Low	N/A	High	Low	Low
Mean	−0.68	−0.51	−0.82	−0.86	−0.26	−0.18	−0.59	−0.34	−0.68	−0.32	−1.53	−0.93
Standard error	0.01	0.01	0.03	0.03	0.01	0.01	0.04	0.02	0.02	0.01	0.06	0.03
Median	−0.61	−0.51	−0.78	−0.82	−0.17	−0.13	−0.57	−0.27	−0.47	−0.21	−1.35	−0.88
Mode	−0.01	−0.01	−0.55	−0.37	0.00	0.00	0.01	0.01	0.00	0.00	−1.46	0.01
Standard deviation	0.46	0.35	0.34	0.54	0.31	0.21	0.47	0.33	0.73	0.35	0.89	0.74
Sample variance	0.21	0.12	0.11	0.29	0.10	0.04	0.22	0.11	0.53	0.13	0.80	0.54
Kurtosis	1.36	−0.20	0.14	0.34	3.73	4.37	−0.48	1.28	2.77	1.62	0.27	0.66
Skewness	−0.97	−0.49	−0.64	−0.80	−1.78	−1.78	−0.48	−1.21	−1.53	−1.32	−0.92	−0.74
Range	2.59	1.73	1.72	2.58	2.01	1.35	1.85	1.74	4.79	1.92	4.24	4.79
Minimum	−2.59	−1.73	−1.73	−2.59	−2.00	−1.35	−1.84	−1.73	−4.78	−1.92	−4.23	−4.78
Maximum	0.00	0.00	−0.01	−0.01	0.01	0.00	0.01	0.01	0.01	0.00	0.01	0.01
Count	1067	544	147	376	1813	1155	176	481	2022	1092	255	675

Study site 2: CAKR	1950 to 1980				1980 to 2003				2003 to 2014			
	ALL	PB	GB	FD	ALL	PB	GB	FD	ALL	PB	GB	FD
Ice content	N/A	Medium	Low	Low	N/A	Medium	Low	Low	N/A	Medium	Low	Low
Mean	−0.04	−0.16	−0.03	0.04	−0.22	−0.30	−0.11	−0.24	−0.13	−0.20	−0.14	0.03
Standard error	0.01	0.01	0.01	0.02	0.01	0.02	0.01	0.03	0.01	0.02	0.02	0.04
Median	−0.05	−0.10	0.00	−0.02	−0.14	−0.20	−0.06	−0.12	−0.06	−0.04	−0.11	0.06
Mode	0.00	0.00	0.00	−0.06	−0.19	0.00	0.02	−0.19	0.00	0.00	−0.23	0.16
Standard deviation	0.34	0.19	0.25	0.30	0.40	0.42	0.29	0.45	0.51	0.44	0.44	0.70
Sample variance	0.12	0.04	0.06	0.09	0.16	0.18	0.08	0.20	0.26	0.19	0.20	0.48
Kurtosis	12.20	3.45	3.98	2.50	12.37	17.84	3.36	1.90	14.54	22.44	19.23	6.00
Skewness	1.95	−1.70	−1.48	−0.06	−2.75	−3.80	−1.31	−1.45	−1.69	−4.38	−2.46	−0.37
Range	3.34	1.02	1.72	2.09	3.83	3.05	2.16	2.53	6.54	3.30	5.57	6.24
Minimum	−1.11	−1.02	−1.11	−1.07	−3.05	−3.05	−1.66	−1.75	−3.57	−3.30	−3.57	−3.27
Maximum	2.23	0.00	0.61	1.02	0.78	0.00	0.50	0.78	2.97	0.00	2.00	2.97
Count	870	377	347	146	1323	579	472	272	1373	506	580	273

Table 4
F-tests of the equality of variances in erosion line change between time slices. F = variance A / variance B; n is the raw sample size, the count of DSAS transects with erosion line data available for both time slices; df is the degrees of freedom adjusted for spatial autocorrelation df = (n / 40) − 1, the factor of 40 accounts for the observed spatial autocorrelation out to a maximum of 2000 m, between DSAS transects spaced at 50 m; p is the two-tailed F-test probability. Note that the variances in Table 3 differ slightly from those in this table because the values in Table 3 include all transects, while this table includes only values for transects which were measured across all time slices.

Time slice A	Time slice B	Variance A	Variance B	F	n	df	p
BELA T3	BELA T1	0.52	0.21	2.50	930	22	0.04
BELA T3	BELA T2	0.45	0.12	3.85	1587	39	0.00
CAKR T3	CAKR T1	0.28	0.10	2.79	1151	28	0.01
CAKR T3	CAKR T2	0.28	0.10	2.85	1151	28	0.01

6.3. Rates of change in NW Alaska compared to elsewhere in the Arctic

The coastal dynamics we describe from the southeast Chukchi Sea are somewhat similar to those described for other Arctic coastlines. Hershel Island in the eastern Beaufort Sea has clastic shorelines of permafrost bluffs and a gravelly spit that exhibit rates of geomorphic change similar to BELA. Between 1950 and 1970, mean rates of shoreline erosion on Hershel Island were $-0.6\,m\,yr^{-1}$, but between 1970 and 2000 rates of erosion slowed to $-0.5\,m\,yr^{-1}$. Between 2000 and 2011, erosion rate increased again to $-1.3\,m\,yr^{-1}$ (Radosavljevic et al., 2016). The rates of barrier-island erosion in BELA are also similar to those observed along the Beaufort Sea coastline of Alaska where exposed barrier islands eroded at an average rate of $-1.3\,m\,yr^{-1}$ between 1980 and 2010 (Gibbs and Richmond, 2017). This is similar to the rates of $-1.53\,m\,yr^{-1}$ along barrier-island shorelines in BELA between 2003 and 2014. Along barrier systems on the Tuktoyuktuk Peninsula in Canada, a slightly more rapid rate of erosion of up to $\sim 3\,m\,yr^{-1}$ occurred between 1950 and 1980 (Hequette and Ruz, 1991).

In contrast to ice-rich permafrost-affected coastlines that are dominated by erosion, recent research on paraglacial coasts in Greenland and Svalbard has described an increase in increased sediment accumulation (Bendixen et al., 2017; Strzelecki et al., 2018). In both these regions, warming since the 1980s has resulted in increased glacial run-off and sediment transport that has contributed to the growth of both deltas (Bendixen et al., 2017) and spit systems (Strzelecki et al., 2018).

Ice-rich permafrost bluffs in our study areas are eroding more slowly than those in other regions. Mean erosion rates of low (< 3 m), ice-rich permafrost bluffs at Drew Point on the Alaska Beaufort Sea coast reached $13.6\,m\,yr^{-1}$ between 2002 and 2007 (Jones et al., 2009), which is 45× faster than the rates we observed in BELA between 2003 and 2014. In the Laptev Sea, erosion rates along 20-meter high, ice-rich permafrost bluffs averaged $-3.4 \pm 2.7\,m\,yr^{-1}$ between 2010 and 2013 (Günther et al., 2015), which is around 10× faster than bluff retreat observed in BELA. These regional variations in coastal erosion can be caused by a variety of factors including the height of the backshore, variations in beach geometry, differences in nearshore bathymetry and sediment budgets, and changes in fetch caused by declining sea-ice cover (Lantuit et al., 2012).

6.4. Trajectories of coastal change in the Chukchi Sea

Although shorelines in the southeast Chukchi Sea have become increasingly dynamic over the last 50 years, they have yet to experience

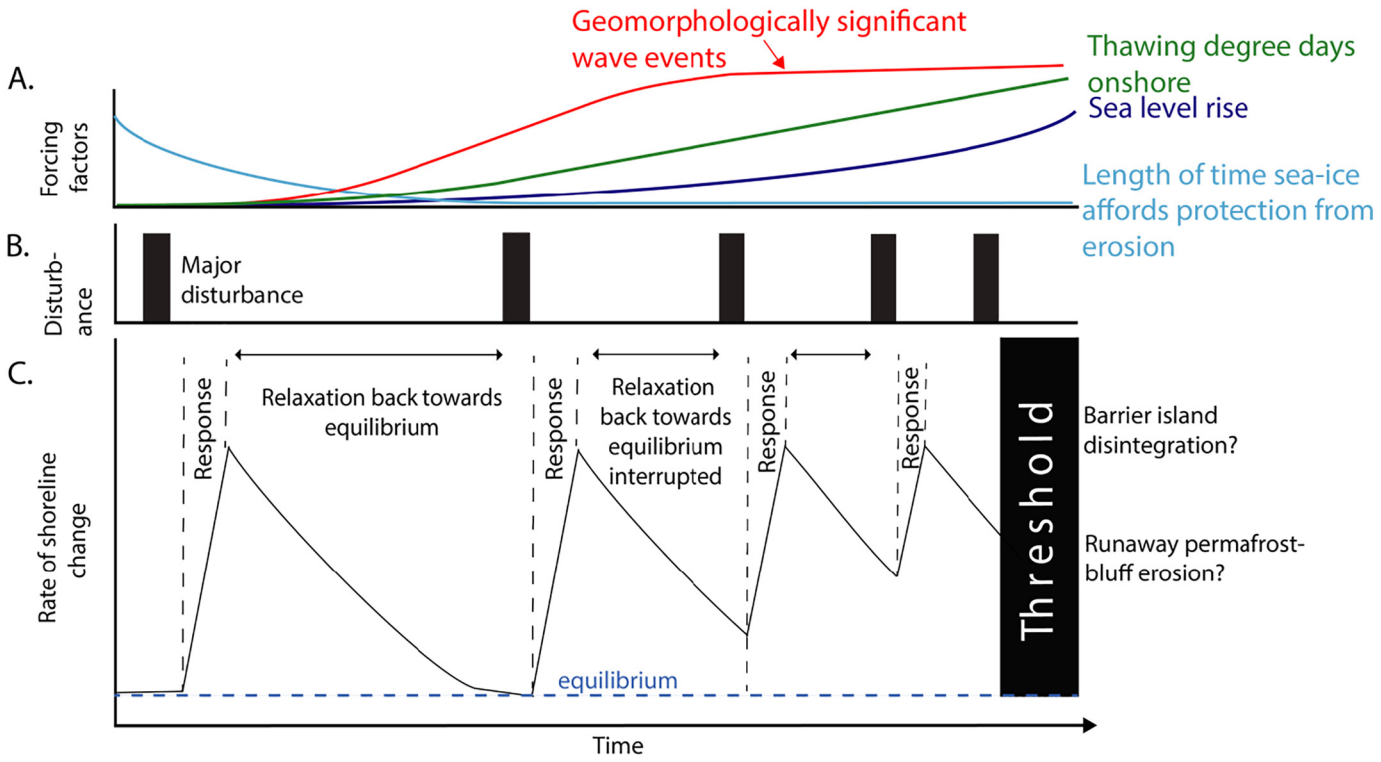

Fig. 9. Conceptual diagram illustrating the potential, cumulative effect of climate change on the study coastlines. A) Key climate change-related factors and their projected changes over the coming century (Stocker et al., 2014, Panda et al., 2016). B) The frequency of disturbance events will increase over the coming century in response to the cumulative impacts of the forcing factors. C) Impact of the disturbance events on coastal geomorphology. While regularly spaced disturbances allow coastal systems to respond and then relax back to equilibria, an increase in the frequency of disturbances reduces the amount of time a system has to regain equilibrium. Eventually this forces a stable coastal system into a new geomorphological state.

significant geomorphological shifts in response to sea-ice decline. The pre-existing late Holocene coastal landforms show no sign of being suddenly altered or radically modified by the changing sea-ice regime. However, we predict that, as the open-water season continues to lengthen, shoreline geomorphic processes in BELA and CAKR will begin to change more rapidly. Shorelines now characterized by erosion will see erosion rates increase, and shorelines now experiencing sediment deposition will accrete even more rapidly.

Shorelines in BELA and CAKR appear to be resilient to not just to changes in the sea-ice regime but also to changes in climate and in RSL; however, it is possible that significant geomorphological thresholds will be crossed in the next 50–100 years (Masselink et al., 2016; Moore et al., 2010; Slott et al., 2006). We infer that these shorelines are being pushed towards major, geomorphic thresholds by five interacting factors: warming ground, air, and ocean temperatures; sea-ice decline; relative sea-level rise; changes in the frequency and tracks of storms; and changes in the wave regime caused by all of the above (Fig. 9). Geomorphic systems tend to recover from disturbance events like severe storms by relaxing back towards their prior, equilibrial states (Woodroffe, 2002); however, if the overall energetic state of a coastline is progressively increasing through time, it may be pushed towards or over a novel geomorphological threshold. In the case of the BELA and CAKR shorelines, we speculate there are two key thresholds: 1) the disintegration of barrier islands in the southwestern reach of the BELA coast caused by increased or interrupted longshore transport combined with rising sea level; and 2) runaway thermokarst erosion of coastal bluffs in BELA as rising sea level and the erosion of barrier islands exposes ice-rich uplands to direct wave action over an increasingly lengthy, ice-free season (Fig. 10).

Barrier islands in southwest BELA presently show the highest erosion rates in the study region, primarily due to sediment erosion and its transport towards the northeast. As the open-water season lengthens, sediment erosion along BELAs barrier islands and transport to the NE will operate over longer intervals. In addition, a rapid rise in sea level will increase the tidal prism, which on the coastline of the eastern USA has led to an increase in the amount of sediment captured in lagoons, leading to the depletion of sand supply for islands further down the barrier island chain. This in turn has starved those downdrift islands of sediment, which triggers increased erosion and results in narrower and more segmented barrier island system (FitzGerald et al., 2008). The fragmentation of barrier islands in BELA could then expose ca.100 km of ice-rich permafrost bluffs to open water and possibly change both the rate of shoreline retreat and the coastal sediment budget.

Once stripped of the protection afforded by the barrier islands, ice-rich permafrost bluffs could experience a positive feedback in the rate of erosion that is unique to polar regions. Typically, shoreline response to rising RSL and/or increased wave attack involves re-equilibration of the entire shoreface profile as the eroded sediment is transferred offshore, where it aggrades vertically and re-establishes the pre-existing equilibrium profile of the shoreface (Bruun, 1962; Are and Reimnitz, 2008). Subsequently, the overall beach profile tends to move landward and upward simultaneously. However, if unconsolidated, ice-rich sediment underlies the supratidal zone, a slight rise in RSL or increase in wave energy can push the shoreline far out of equilibrium because the melting ice deflates the ground surface without supplying the lower shoreface with sediment (Fig. 10). As a result, shoreline retreat needs to continue much farther inland in order to acquire sufficient sediment to re-establish an equilibrium profile. It follows that although Arctic beach/shoreface profiles conform to the same power function as lower latitude coasts (Are and Reimnitz, 2008), their rate of retreat in response to the same increase of RSL or wave attack may be far greater. While shoreline response will likely be complicated further by the influence of sea-ice and permafrost on sediment availability and sediment transport capacity, this conceptual framework provides a useful

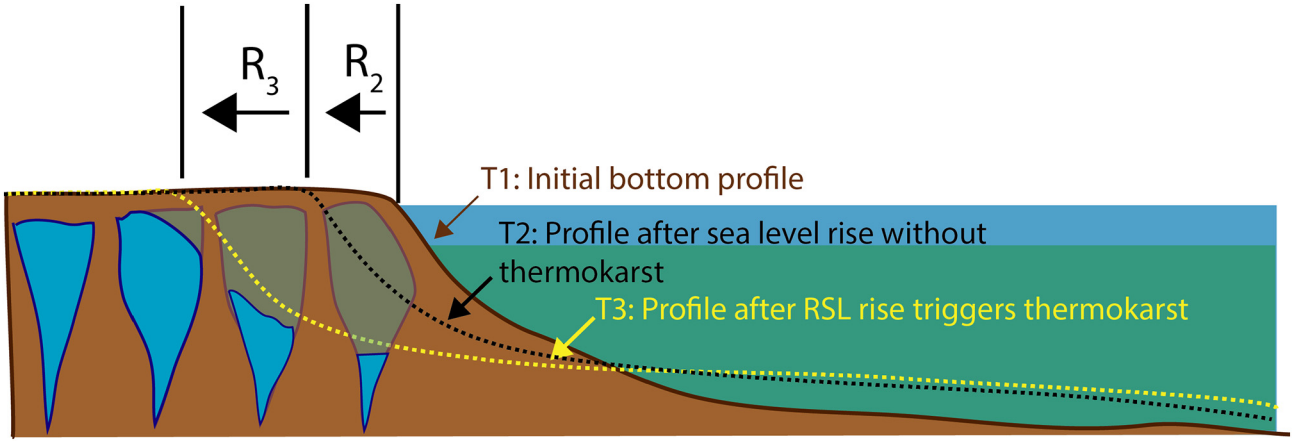

Fig. 10. Conceptual model of thermokarst-accentuated Bruun retreat along an ice-rich, permafrost-affected shoreline. In the absence of ground ice, a rise in sea level results in a relatively small amount of landward movement (R_2, corresponding with T2). In contrast, the scenario in red shows how the presence of ground ice results in the sea moving further landward (R_3, corresponding with T2). (For interpretation of the references to color in this figure legend, the reader is referred to the web version of this article.)
Modified from FitzGerald et al. (2008).

platform to explore potential trajectories of coastal change. This thermokarst-accentuated retreat may underlie the rapid retreat of ice-rich bluffs now underway along the Beaufort Sea where erosion rates currently exceed 13 m yr^{-1} (Jones et al., 2009). If ice-rich yedoma bluffs in BELA lose their sheltering barrier islands, they could experience similarly rapid rates of retreat.

7. Conclusions

This study quantifies the temporal and spatial patterns of geomorphic change along an Arctic coastline that is rapidly losing its sea-ice cover. Results illustrate the geomorphic and temporal complexity of coastal responses to ongoing climate change during the past 60+ years. Specifically:

- Sea-ice cover in this part of the Chukchi Sea has decreased ~10 days per decade since satellite observations began in 1979, and the increasing duration of open water has led to an increase in the amount of wave energy available for sediment erosion and transport on and along the shoreline.
- Coastal geomorphology is changing more rapidly in recent years due to increased rates of both erosion and accumulation. The extent of these changes varies markedly between different coastal reaches and landforms. Low-lying shorelines of sandy barrier islands in BELA experienced a net change of -1.53 m yr^{-1} between 2003 and 2014. In contrast, gravel barrier beaches in CAKR are more stable, changing at a mean rate of -0.13 m yr^{-1}. Rates of change along ice-rich permafrost bluffs in BELA were -0.3 m yr^{-1} during the 2003–2014 period, which is slow compared to other shoreline types in the study area and to shorelines with similar geomorphologies in other regions of the Arctic (Günther et al., 2015; Jones et al., 2009).
- To better predict coastal change in the southeastern Chukchi Sea, beach processes need to be tied to environmental forcing factors with more confidence. This requires investigations of geomorphic changes at an annual to sub-annual time scales both onshore and in the subtidal zone.

Acknowledgements

This study was funded by a National Park Service cooperative agreement P14AC01135 and by National Science Foundation, Arctic Natural Sciences grant 1417611 and Polar Programs Grant 1745369. We thank China Kantner and Sara Grocott for field assistance, and Seth Kantner for advice on field safety. Chris Maio, Jacqueline Overbeck, and Nicole Kinsman provided useful discussions in the course of this work. Suggestions from two anonymous reviewers greatly improved this manuscript.

Appendix A. Supplementary data

Supplementary data to this article can be found online at https://doi.org/10.1016/j.margeo.2018.07.007.

References

AMAP, 2012. Arctic climate issues 2011: changes in Arctic snow, water, ice and permafrost, SWIPA 2011 overview report. In: Arctic Monitoring and Assessment Programme (AMAP), . https://doi.org/ISBN978-82-7971-073-8.
Are, F.E., 1988. Thermal abrasion of sea coasts. Polar Geogr. Geol 12, 87–155.
Are, F., Reimnitz, E., 2008. The *A* and *m* coefficients in the Bruun/Dean equilibrium profile equation seen from the Arctic. J. Coast. Res. 2, 243–249. https://doi.org/10.2112/05-0572.1.
Barnhart, K.R., Anderson, R.S., Overeem, I., Wobus, C., Clow, G.D., Urban, F.E., 2014a. Modeling erosion of ice-rich permafrost bluffs along the Alaskan Beaufort Sea coast. J. Geophys. Res. Earth Surf. 119, 1155–1179. https://doi.org/10.1002/2013JF002845.
Barnhart, K.R., Overeem, I., Anderson, R.S., 2014b. The effect of changing sea ice on the physical vulnerability of Arctic coasts. Cryosphere 8, 1777–1799. https://doi.org/10.5194/tc-8-1777-2014.
Belchansky, G.I., Douglas, D.C., Platonov, N.G., 2004. Duration of the Arctic sea ice melt season: regional and interannual variability, 1979–2001. J. Clim. 17, 67–80. https://doi.org/10.1175/1520-0442(2004)017<0067:DOTASI>2.0.CO;2.
Bendixen, M., Iversen, L.L., Bjørk, A.A., Elberling, B., Westergaard-Nielsen, A., Overeem, I., Barnhart, K.R., Khan, S.A., Box, J.E., Abermann, J., 2017. Delta progradation in Greenland driven by increasing glacial mass loss. Nature 550, 101.
Blier, W., Keefe, S., Shaffer, W.A., Kim, S.C., 1997. Storm surges in the region of western Alaska. Mon. Weather Rev. 125, 3094–3108.
Boak, E.H., Turner, I.L., 2005. Shoreline definition and detection: a review. J. Coast. Res. https://doi.org/10.2112/03-0071.1.
Bowman, A.W., Azzalini, A., 2014. R Package "sm": Nonparametric Smoothing Methods (Version 2.2-5.4).
Bowman, A.W., Crujeiras, R.M., 2013. Inference for variograms. Comput. Stat. Data Anal. 66, 19–31. https://doi.org/10.1016/j.csda.2013.02.027.
Bruun, P., 1962. Sea-level rise as a cause of shore erosion. In: Proceedings of the American Society of Civil Engineers, pp. 117–130.
Cavalieri, D., Parkinson, C., Gloersen, P., Zwally, H.J., 1996. Sea ice concentrations from Nimbus-7 SMMR and DMSP SSM/I passive microwave data. National Snow and Ice Data Center. Boulder, Colorado, USA.
Cohen, J., Screen, J.A., Furtado, J.C., Barlow, M., Whittleston, D., Coumou, D., Francis, J., Dethloff, K., Entekhabi, D., Overland, J., Jones, J., 2014. Recent Arctic amplification and extreme mid-latitude weather. Nat. Geosci. https://doi.org/10.1038/ngeo2234.
Dolan, R., Fenster, M.S., Holme, S.J., 1991. Temporal analysis of shoreline recession and accretion. J. Coast. Res. 7, 723–744.
Elias, S.A., Short, S.K., Nelson, C.H., Birks, H.H., 1996. Life and times of the Bering land bridge. Nature 382, 60–63. https://doi.org/10.1038/382060a0.
Farquharson, L., Anthony, K.W., Bigelow, N., Edwards, M., Grosse, G., 2016. Facies analysis of yedoma thermokarst lakes on the northern Seward Peninsula, Alaska. Sediment. Geol. https://doi.org/10.1016/j.sedgeo.2016.01.002.

Fathauer, T.F., 1978. A Forecast Procedure for Coastal Floods in Alaska. National Weather Service, Regional Headquarters, US Department of Commerce, National Oceanic and Atmospheric Administration.
Fitzgerald, D.M., Fenster, M.S., Argow, B.A., Buynevich, I.V., 2008. Coastal impacts due to sea-level rise. Annu. Rev. Earth Planet. Sci. 36, 601–647. https://doi.org/10.1146/annurev.earth.35.031306.140139.
Forbes, D.L., 2011. State of the Arctic coast 2010 – scientific review and outlook. In: International Arctic Science Committee, Land-ocean Interactions in the Coastal Zone, Arctic Monitoring and Assessment Programme, International Permafrost Association. Helmholtz-Zentrum, Geesthacht, Germany (178 pp.).
Francis, O.P., Panteleev, G.G., Atkinson, D.E., 2011. Ocean wave conditions in the Chukchi Sea from satellite and in situ observations. Geophys. Res. Lett. 38. https://doi.org/10.1029/2011GL049839.
Gibbs, A.E., Richmond, B.M., 2017. National assessment of shoreline change—summary statistics for updated vector shorelines and associated shoreline change data for the north coast of Alaska. In: US-Canadian Border to Icy Cape. US Geological Survey.
Gorokhovich, Y., Leiserowiz, A., 2012. Historical and future coastal changes in Northwest Alaska. J. Coast. Res. 28, 174–186.
Günther, F., Overduin, P.P., Sandakov, A.V., Grosse, G., Grigoriev, M.N., 2013. Short- and long-term thermo-erosion of ice-rich permafrost coasts in the Laptev Sea region. Biogeosciences 10, 4297–4318. https://doi.org/10.5194/bg-10-4297-2013.
Günther, F., Overduin, P.P., Yakshina, I.A., Opel, T., Baranskaya, A.V., Grigoriev, M.N., 2015. Observing Muostakh disappear: permafrost thaw subsidence and erosion of a ground-ice-rich island in response to arctic summer warming and sea ice reduction. Cryosphere 9, 151–178. https://doi.org/10.5194/tc-9-151-2015.
Harper, J.R., 1990. Morphology of the Canadian Beaufort Sea coast. Mar. Geol. 91, 75–91. https://doi.org/10.1016/0025-3227(90)90134-6.
Hequette, A., Barnes, P.W., 1990. Coastal retreat and shoreface profile variations in the Canadian Beaufort Sea. Mar. Geol. 91, 113–132. https://doi.org/10.1016/0025-3227(90)90136-8.
Hequette, A., Ruz, M.H., 1991. Spit and Barrier-Island Migration in the Southeastern Canadian Beaufort Sea. J. Coast. Res. 7, 677–698.
Hopkins, D.M., 1973. Sea level history in Beringia during the past 250,000 years. Quat. Res. 3, 520–540. https://doi.org/10.1016/0033-5894(73)90029-X.
Hopkins, D.M., 1977. Coastal Processes and Coastal Erosional Hazards to the Cape Krusenstern Archaeological Site. US Geological Survey.
Hume, J.D., Schalk, M., 1967. Shoreline processes near Barrow, Alaska: a comparison of the normal and the catastrophic. Arctic 86–103.
Jones, B.M., Arp, C.D., Jorgenson, M.T., Hinkel, K.M., Schmutz, J.A., Flint, P.L., 2009. Increase in the rate and uniformity of coastline erosion in Arctic Alaska. Geophys. Res. Lett. 36, L03503. https://doi.org/10.1029/2008gl036205.
Jordan, J.W., Mason, O.K., 1999. A 5000 year record of intertidal peat stratigraphy and sea level change from northwest Alaska. Quat. Int. https://doi.org/10.1016/S1040-6182(99)00005-1.
Jorgenson, M.T., Brown, J., 2005. Classification of the Alaskan Beaufort Sea Coast and estimation of carbon and sediment inputs from coastal erosion. Geo-Mar. Lett. 25, 69–80.
Kasprzak, M., Strzelecki, M.C., Traczyk, A., Kondracka, M., Lim, M., Migała, K., 2017. On the potential for a bottom active layer below coastal permafrost: the impact of sea-water on permafrost degradation imaged by electrical resistivity tomography (Hornsund, SW Spitsbergen). Geomorphology 293, 347–359.
Komar, P.D., 1998. Beach Processes and Sedimentation, 2nd ed. Prentice-Hall.
Lantuit, H., Pollard, W.H., 2008. Fifty years of coastal erosion and retrogressive thaw slump activity on Herschel Island, southern Beaufort Sea, Yukon Territory, Canada. Geomorphology 95, 84–102.
Lantuit, H., Overduin, P.P., Couture, N., Wetterich, S., Aré, F., Atkinson, D., Brown, J., Cherkashov, G., Drozdov, D., Lawrence Forbes, D.L., Graves-Gaylord, A., Grigoriev, M., Hubberten, H., Jordan, J., Jorgenson, T., Ødegård, R.S., Ogorodov, S., Pollard, W.H., Rachold, V., Sedenko, S., Solomon, S., Steenhuisen, F., Streletskaya, I., Vasiliev, A., 2012. The Arctic coastal dynamics database: a new classification scheme and statistics on Arctic permafrost coastlines. Estuar. Coasts 35, 383–400. https://doi.org/10.1007/s12237-010-9362-6.
Lawrence, D.M., Slater, A.G., 2005. A projection of severe near-surface permafrost degradation during the 21st century. Geophys. Res. Lett. 32, 1–5. https://doi.org/10.1029/2005GL025080.
Lentz, E.E., Hapke, C.J., Stockdon, H.F., Hehre, R.E., 2013. Improving understanding of near-term barrier island evolution through multi-decadal assessment of morphologic change. Mar. Geol. 337, 125–139. https://doi.org/10.1016/j.margeo.2013.02.004.
Lenz, J., Grosse, G., Jones, B.M., Walter Anthony, K.M., Bobrov, A., Wulf, S., Wetterich, S., 2016. Mid-Wisconsin to Holocene permafrost and landscape dynamics based on a drained lake basin core from the northern Seward Peninsula, Northwest Alaska. Permafr. Periglac. Process. 27, 56–75. https://doi.org/10.1002/ppp.1848.
MacCarthy, G.R., 1953. Recent changes in the shoreline near Point Barrow, Alaska. Arctic 6, 44–51.
Mahoney, A.R., Eicken, H., Gaylord, A.G., Gens, R., 2014. Landfast sea ice extent in the Chukchi and Beaufort Seas: the annual cycle and decadal variability. Cold Reg. Sci. Technol. 103, 41–56. https://doi.org/10.1016/j.coldregions.2014.03.003.
Manley, W.F., Lestak, L.R., 2012. Protocol for High-resolution Geospatial Analysis of Coastal Change in the Arctic Network of Parks. National Park Service, Fort Collins, Colorado.
Manley, W.F., Jordan, J.W., Lestak, L.R., Mason, O.K., 2007. Coastal change since 1950 in the southeast Chukchi Sea, Alaska, based on GIS and field measurements. In: Arctic Coastal Zones at Risk Workshop in Tromso, Norway.
Manley, W.F., Parrish, E.G., Sanzone, D.M., Lestak, L.R., 2007a. High-resolution Orthorectified Imagery From Approximately 1950 for the Coastal Areas of Bering Land Bridge NP (BELA) and Cape Krusenstern NM (CAKR), Northwest Alaska, Report, Arctic Network Invent. and Monit. Program, Natl. Park Serv., Fairbanks, Alaska.
Manley, W.F., Sanzone, D.M., Lestak, L.R., Parrish, E.G., 2007b. High-resolution Orthorectified Imagery From Approximately 1980 for the Coastal Areas of Bering Land Bridge NP (BELA) and Cape Krusenstern NM (CAKR), Northwest Alaska.
Manley, W.F., Sanzone, D.M., Lestak, L.R., Parrish, E.G., 2007c. High-resolution Orthorectified Imagery From 2003 for the Coastal Areas of Bering Land Bridge NP (BELA) and Cape Krusenstern NM (CAKR), Northwest Alaska, Report, Arctic Network Invent. and Monit. Program, Natl. Park Serv., Fairbanks, Alaska.
Mars, J.C., Houseknecht, D.W., 2007. Quantitative remote sensing study indicates doubling of coastal erosion rate in past 50 yr along a segment of the Arctic coast of Alaska. Geology 35. https://doi.org/10.1130/G23672A.
Mason, O.K., Jordan, J.W., 1993. Heightened North Pacific storminess during synchronous late Holocene erosion of northwest Alaska beach ridges. Quat. Res. 40, 55–69.
Mason, O.K., Jordan, J.W., Plug, L., 1995. Late Holocene storm and sea-level history in the Chukchi Sea. J. Coast. Res. 173–180.
Mason, O.K., Salmon, D.K., Ludwig, S.L., 1996. The periodicity of storm surges in the Bering Sea from 1898 to 1993, based on newspaper accounts. Clim. Chang. 34, 109–123.
Mason, O.K., Hopkins, D.M., Plug, L., 1997. Chronology and paleoclimate of storm-induced erosion and episodic dune growth across Cape Espenberg Spit, Alaska, U.S.A. J. Coast. Res. 13 (3), 770–797.
Masselink, G., Castelle, B., Scott, T., Dodet, G., Suanez, S., Jackson, D., Floc'H, F., 2016. Extreme wave activity during 2013/2014 winter and morphological impacts along the Atlantic coast of Europe. Geophys. Res. Lett. 43, 2135–2143. https://doi.org/10.1002/2015GL067492.
Miller, G.H., Alley, R.B., Brigham-Grette, J., Fitzpatrick, J.J., Polyak, L., Serreze, M.C., White, J.W.C., 2010. Arctic amplification: can the past constrain the future? Quat. Sci. Rev. 29, 1779–1790. https://doi.org/10.1016/j.quascirev.2010.02.008.
Moore, L.J., List, J.H., Williams, S.J., Stolper, D., 2010. Complexities in barrier island response to sea level rise: insights from numerical model experiments, North Carolina Outer Banks. J. Geophys. Res. 115, F03004. https://doi.org/10.1029/2009JF001299.
Overeem, I., Anderson, R.S., Wobus, C.W., Clow, G.D., Urban, F.E., Matell, N., 2011. Sea ice loss enhances wave action at the Arctic coast. Geophys. Res. Lett. 38. https://doi.org/10.1029/2011GL048681.
Panda, S., Romanovsky, V., Marchenko, S., 2016. High-resolution Permafrost Modeling in the Arctic Network National Parks, Preserves and Monuments. https://doi.org/10.13140/RG.2.2.18127.89767.
R Development Core Team, 2016. R: A Language and Environment for Statistical Computing. 0 R Found. Stat. Comput., Vienna Austria. https://doi.org/10.1038/sj.hdy.6800737. ({ISBN} 3-900051-07-0).
Radosavljevic, B., Lantuit, H., Pollard, W., Overduin, P., Couture, N., Sachs, T., Helm, V., Fritz, M., 2016. Erosion and flooding—threats to coastal infrastructure in the Arctic: a case study from Herschel Island, Yukon Territory, Canada. Estuar. Coasts 39, 900–915. https://doi.org/10.1007/s12237-015-0046-0.
Rasmussen, E.A., Turner, J., Thorpe, A.J., 2004. Polar lows: mesoscale weather systems in the polar regions. Q. J. R. Meteorol. Soc. 130, 371–372.
Romanovsky, V.E., Smith, S.L., Shiklomanov, N.I., Streletskiy, D.A., Isaksen, K., Kholodov, A.L., Christiansen, H.H., Drozdov, D.S., Malkova, G.V., Marchenko, S.S., 2017. Terrestrial permafrost. In: Blunden, J., Arndt, D. (Eds.), State of the Climate in 2016. Bulletin of the American Meteorological Societypp. ES1–ES32.
Serreze, M.C., Barry, R.G., 2011. Processes and impacts of Arctic amplification: a research synthesis. Glob. Planet. Chang. 77, 85–96. https://doi.org/10.1016/j.gloplacha.2011.03.004.
Slott, J.M., Murray, A.B., Ashton, A.D., Crowley, T.J., 2006. Coastline responses to changing storm patterns. Geophys. Res. Lett. 33. https://doi.org/10.1029/2006GL027445.
Solomon, S.M., 2005. Spatial and temporal variability of shoreline change in the Beaufort-Mackenzie region, northwest territories, Canada. Geo-Mar. Lett. 25, 127–137.
Stive, M.J.F., Aarninkhof, S.G.J., Hamm, L., Hanson, H., Larson, M., Wijnberg, K.M., Nicholls, R.J., Capobianco, M., 2002. Variability of shore and shoreline evolution. Coast. Eng. 47, 211–235. https://doi.org/10.1016/S0378-3839(02)00126-6.
Stocker, T., Stocker, T.F., Qin, D., Plattner, G.K., Tignor, M., Allen, S.K., Boschung, J., Nauels, A., Xia, Y., Bex, V., Midgley, P.M., 2014. Climate Change 2013: The Physical Science Basis: Working Group I Contribution to the Fifth Assessment Report of the Intergovernmental Panel on Climate Change.
Strzelecki, M.C., Long, A.J., Lloyd, J.M., Małecki, J., Zagórski, P., Pawłowski, Ł., Jaskólski, M.W., 2018. The role of rapid glacier retreat and landscape transformation in controlling the post-L ittle I ce A ge evolution of paraglacial coasts in central S pitsbergen (B illefjorden, S valbard). Land Degrad. Dev. 29 (6), 1962–1978.
Thieler, E.R., Himmelstoss, E.A., Zichichi, J.L., Ergul, A., 2009. The Digital Shoreline Analysis System (DSAS) Version 4.0—An ArcGIS Extension for Calculating Shoreline Change. US Geological Survey.
Thomson, J., Rogers, W.E., 2014. Swell and sea in the emerging Arctic Ocean. Geophys. Res. Lett. 41, 3136–3140. https://doi.org/10.1002/2014GL059983.
Thomson, J., Fan, Y., Stammerjohn, S., Stopa, J., Rogers, W.E., Girard-Ardhuin, F., Ardhuin, F., Shen, H., Perrie, W., Shen, H., Ackley, S., Babanin, A., Liu, Q., Guest, P., Maksym, T., Wadhams, P., Fairall, C., Persson, O., Doble, M., Graber, H., Lund, B., Squire, V., Gemmrich, J., Lehner, S., Holt, B., Meylan, M., Brozena, J., Bidlot, J.R., 2016. Emerging trends in the sea state of the Beaufort and Chukchi seas. Ocean Model 105, 1–12. https://doi.org/10.1016/j.ocemod.2016.02.009.
Timmermans, M.L., Proshutinsky, A., 2015. Sea surface temperature. In: Blunden, J., Arndt, D. (Eds.), State of the Climate in 2014. Bulletin of the American Meteorological Societypp. ES1–ES32.
Wang, M.Y., Overland, J.E., 2009. A sea ice free summer Arctic within 30 years? Geophys. Res. Lett. 36, L07502. https://doi.org/10.1029/2009GL037820.
Woodroffe, C.D., 2002. Coasts: Form, Process and Evolution. Cambridge University Press.